European Journal of Advanced Chemistry Research
Vol 6 | Issue 3 | November 2025
ISSN 2684-4478

RESEARCH ARTICLE

Targeted Detection of Low-Level Chlorpyrifos Residues in Milk Using Chemometrics-Aided Raman Spectroscopy

J. M. Thuku[1,2,*], M. I. Kaniu[2], C. N. Ndung'u[2], L. W. Kiruri[1], and K. A. Kaduki[2]

ABSTRACT

Contamination of milk with pesticide residues such as chlorpyrifos poses serious public health concerns, necessitating highly sensitive analytical tools for effective monitoring. Raman spectroscopy offers a non-invasive and practical detection method; however, conventional full-spectrum or broad-region analyses often fail to reliably detect low-level residues due to spectral overlap and matrix interference. This study demonstrates that surface-enhanced Raman spectroscopy, combined with chemometric techniques (ANOVA and PCA), can establish a selective molecular fingerprint for chlorpyrifos, enabling accurate detection even at concentrations below the maximum residue limit (MRL) of 0.01 ppm. Spectra were acquired from both pesticide-free milk and samples spiked at various chlorpyrifos concentrations. ANOVA identified statistically significant spectral differences at 342, 572, 634, 736, 1378, and 1568 cm^{-1}, with the greatest variance observed in the 314–750 cm^{-1} range. PCA revealed that the 314–354 cm^{-1} band, centered at 342 cm^{-1} and corresponding to the C–Cl stretching mode unique to chlorpyrifos, served as the most reliable molecular fingerprint. This band was absent in the milk matrix, allowing clear differentiation across contamination levels. These findings support a targeted fingerprinting strategy that minimizes spectral interference and enhances sensitivity for trace-level detection, offering a rapid, robust, and cost-effective tool for pesticide monitoring in milk. The method holds promise for broader application in food safety surveillance and regulatory compliance.

Keywords: Chlorpyrifos detection, Food safety, Principal component analysis, Raman spectroscopy.

Submitted: September 11, 2025

Published: November 14, 2025

10.24018/ejchem.2025.6.3.165

[1] *Department of Chemistry, Kenyatta University, Nairobi, Kenya.*
[2] *Department of Physics, University of Nairobi, Nairobi, Kenya.*

* ***Corresponding Author:***
e-mail: jeremythuku@gmail.com

1. Introduction

Chlorpyrifos, a chlorinated organophosphorus pesticide, is widely used in developing countries for pest management, including the control of livestock parasites such as ticks [1], [2]. Its environmental persistence, governed by factors such as pH and temperature, results in a reported half-life of 10–120 days [3], [4] which contributes to its bioaccumulation in ecosystems and potential transfer to animal-derived food products. In particular, when used as an acaricide, chlorpyrifos tends to accumulate in adipose tissues and subsequently migrate into milk because of its lipophilicity [5]. Additional contamination pathways include the direct spraying of animal shelters and ingestion of contaminated feed or water [6]. As such, milk is a critical vector for chlorpyrifos exposure among consumers, raising substantial public health concerns about food safety given the compound's well-documented health risks [5], [7].

In recognition of these risks, the European Union has established a stringent maximum residue limit (MRL) of 0.01 ppm for chlorpyrifos in milk [8]. However, several studies have reported chlorpyrifos

concentrations exceeding this regulatory threshold in milk. For instance, Adum *et al*. [1] used high-performance liquid chromatography (HPLC) to quantify chlorpyrifos in milk at concentrations ranging from 1 to 2.854 ppm. Dasriya *et al*. [9] employed gas chromatography-tandem mass spectrometry (GC-MS/MS) and detected levels as low as 0.00347 ppm, whereas Dallegrave *et al*. [10] reported values as high as 0.0457 ppm using a similar analytical technique. Shaker and Elsharkawy [11] found an average concentration of 3.01 ppm using gas chromatography-mass spectrometry (GC-MS). These findings underscore the widespread presence of chlorpyrifos in dairy products and the need for sensitive detection methods.

Although wet chemistry techniques such as HPLC, GC-MS/MS, and GC-MS are considered the gold standards for pesticide residue analysis due to their high sensitivity and reliability, they have significant limitations. These include destructive and complex sample preparation, long processing times, high labor costs, and the need for a specialized laboratory infrastructure [12]. Such constraints limit their suitability for large-scale, on-site, or field-based testing, particularly in resource-limited settings [13].

In contrast, vibrational spectroscopy, particularly Raman spectroscopy, offers a promising non-destructive, cost-effective, and rapid approach for the analysis of chemical residues, with the added advantage of high molecular specificity based on a compound's unique vibrational fingerprint [14]. Unlike infrared spectroscopy, Raman scattering is largely unaffected by the water content in biological matrices and typically requires minimal or no sample preparation [15]–[17]. Nevertheless, Raman signals are inherently weak [18], with only one in every 10^8 incident photons undergoing inelastic scattering [19]. To address this limitation, surface-enhanced Raman spectroscopy (SERS) has been developed to, enable the detection of analytes at trace levels [20], [21]. However, traditional SERS methods require costly and complex nanoparticle synthesis and additional sample preparation, making them less ideal for routine applications in resource-constrained settings [22]. Further, Raman spectra from complex biological matrices such as milk are difficult to interpret due to overlapping bands associated with various biomolecular components [23]–[25]. These challenges highlight the need for chemometric tools that support spectral preprocessing, feature extraction, and statistical discrimination of subtle variations between related sample classes [16], [24], [26].

Milk is a complex matrix composed of proteins, fats, and lactose, and yields intricate Raman spectra owing to the distinct molecular vibrational modes of each constituent [27]. These components give rise to multiple overlapping bands that complicate interpretation, especially when extrinsic compounds such as pesticides introduce additional vibrational features. Hence, identifying a unique molecular fingerprint of chlorpyrifos in milk is essential for reliable and targeted detection. Molecular fingerprinting involves identifying characteristic vibrational bands that reflect the structure and bonding environment of a molecule [28]. While the conventional Raman fingerprint region typically lies below 1500 cm^{-1}, in this study, "molecular fingerprint" refers to the most distinct chlorpyrifos-associated band that allows unambiguous identification. Isolating such a band requires the identification of chlorpyrifos-specific spectral features that differentiate spiked samples from uncontaminated ones. Although Raman spectroscopy has not previously been applied to directly detect chlorpyrifos in milk, it has been used with chemometrics to detect the compound in fruits and vegetables [29], [30]. However, these earlier studies often relied on broad spectral regions, which included non-specific features, reducing the detection performance at low chlorpyrifos concentrations.

This study demonstrates the application of chemometric techniques, that is, analysis of variance (ANOVA) and principal component analysis (PCA), to Raman spectra to identify a specific chlorpyrifos fingerprint in milk, a representative complex biological matrix. We show that targeted band selection improves sensitivity and specificity compared to full-spectrum or broad-region analytical approaches, particularly at concentrations near the MRL of 0.01 ppm. The proposed strategy offers a rapid, analytically robust, and cost-effective method for detecting chlorpyrifos in milk, thereby addressing a critical gap in the current pesticide monitoring practices.

2. Materials and Methods

2.1. Sample Preparation and Raman Data Acquisition

A commercial-grade formulation comprising 50% chlorpyrifos and 50% inert constituents, including surfactants, solvents, and stabilizers, was obtained from a local retail outlet. Fresh, chemical-free milk was sourced from a nomadic pastoralist community in a remote village in Kenya, where livestock exclusively graze on native vegetation without exposure to commercial feed, agrochemicals, or veterinary pesticides. These communities largely do not practice crop farming and avoid the use of synthetic agricultural inputs, thereby minimizing the common environmental pathways for pesticide contamination. Based on this unique ecological and cultural context, the milk used in this study was

deemed a suitable pesticide-free matrix for the controlled spiking experiments. After collection, the milk was immediately transported to the laboratory under controlled conditions in clean, sterilized, and sealed glass bottles to prevent contamination. To reduce potential spectral interference, the milk underwent microfiltration through a 1.4 μm membrane to remove particulate matter and large molecules such as fat globules and protein aggregates [31], [32]. The filtered milk was divided into two groups: a control group and a treatment group. The treatment group was spiked with commercial-grade chlorpyrifos at concentrations of 0.003 ppm (below MRL), 0.01 ppm (MRL), and 0.03 ppm (above MRL). An additional sample containing a high concentration of 1000 ppm chlorpyrifos was prepared to amplify the spectral differences between the control and treated groups.

Aliquots of 50 μL were deposited onto aluminum-wrapped glass slide substrates to enhance signal reflectivity and spectral stability. Aluminum foil was selected as a cost-effective SERS substrate because of its accessibility, affordability, and capacity to enhance Raman signals [33]. Compared with nanoparticle-based substrates, aluminum provides consistent signal amplification with minimal background interference [34], [35]. Raman spectra were acquired using a portable Raman spectrometer (EZRaman-NP-785, Enwave Optronics, Inc.) equipped with a 785 nm excitation laser operating at 300 mW power. The system had a spectral range of 200–2000 cm^{-1} and resolution of 1.290 cm^{-1}. Calibration was performed using a polystyrene reference standard. Before analysis, the spectra of 50% chlorpyrifos and a blank aluminum-wrapped glass slide substrate were collected for comparison and background subtraction, respectively. For each milk sample, spectral data were recorded at 20 randomly selected locations. Each point was acquired with an integration time of 10 s, boxcar width of 1, and averaged over 10 consecutive scans. The total acquisition time for a single spectrum was approximately two minutes.

2.2. *Spectral Data Preprocessing and Analysis*

Baseline correction was performed automatically using a Raman spectrometer during the acquisition. This procedure involved fitting a least-squares line to each region, subtracting it from the signal, and aligning the baseline to near zero, effectively minimizing the broad fluorescence background. Following the acquisition, the raw spectra were subjected to a series of preprocessing steps, including third-order Savitzky-Golay smoothing, multiplicative scatter correction (MSC), and min-max normalization to a range between one and zero [36], [37]. To identify the spectral regions exhibiting the greatest variance attributable to chlorpyrifos, one-way ANOVA [38] was applied to the preprocessed spectra from the control group and 1000 ppm chlorpyrifos-spiked group. For each Raman shift, the variance (σ^2) was calculated based on the intensity differences between the two groups, using the following expression:

$$\sigma^2 = \frac{1}{N-1}\sum_{i=1}^{N}\left(D_i - \overline{D}\right)^2$$

where D_i is the difference between the treated and control spectral intensities at a given Raman shift, $\overline{D}$ is the mean difference at that shift, and N is the number of samples per group. This measure reflects the spread of between-group differences in spectral intensity, with larger values indicating higher variability attributable to chlorpyrifos. To assess statistical significance, these computed variances were incorporated into an ANOVA framework that evaluates the ratio of between-group variance (S_B^2) to within-group variance (S_w^2), expressed by the F-statistic:

$$F = \frac{S_B^2}{S_W^2}$$

The within-group variance was obtained by calculating the individual variances within each group for each Raman shift. An F-test was then performed at each shift to assess relative spectral variance between groups using a p-value threshold of 0.05 to determine statistical significance. Spectral intervals showing significant between-group variance were considered to have potential discriminatory power and subsequently used to guide the selection of key spectral bands for further chemometric analysis.

Statistically significant intervals identified through ANOVA were then used to guide dimensionality reduction via PCA, allowing for exploratory analysis and visualization of spectral differences among sample groups. PCA was performed on both the full spectral range and the regions of interest identified through ANOVA. Principal components were selected based on their contribution to the total explained variance, with the first two components retained for interpretation, as they captured the majority of meaningful spectral variation. PC3 was excluded from further analysis because it accounted for only a marginal proportion of additional variance. All statistical analyses were conducted using the open-source R statistical environment [39], with PCA implemented using the Chemospec package [40].

3. Results and Discussion

3.1. *Spectra of Control and Chlorpyrifos-Spiked Milk*

Fig. 1 shows the average Raman spectra for the control sample and milk spiked with chlorpyrifos at three levels: below the MRL (0.003 ppm), at the MRL (0.01 ppm), and above the MRL (0.03 ppm). Notably, the spectra of the control and low-concentration groups were visually similar in terms of overall band structure and relative intensities. Across all the samples, Raman bands were observed within the spectral range of 354–1742 cm^{-1}. This overlap limits the visual discrimination between groups and highlights the need for multivariate statistical analyses.

The Raman bands and their molecular assignments are summarized in Table I. In addition to carbon and hydrogen, natural cow milk contains several heteroatoms. Nitrogen is mainly present in protein-associated amide groups [27], [41], whereas phosphorus is found in phospholipids [42], [43]. Sulfur is present in amino acids such as cysteine and methionine [44]–[46], and oxygen is abundant in the ester functional groups of fatty acids [43], [47]. These constituents contribute to the complex vibrational modes that form the Raman spectrum of milk.

3.2. *ANOVA of Spectra from Control and 1000 ppm Spiked Groups*

The one-way ANOVA results revealed distinct spectral regions where the variance between the control and 1000 ppm spiked samples was statistically significant. Fig. 2a presents the mean spectra of the control and 1000 ppm chlorpyrifos-spiked milk samples, along with their calculated variance across the full spectral range. Notably, several regions exhibited elevated variances corresponding to chlorpyrifos-associated bands. A reference spectrum of 50% chlorpyrifos was included to confirm that the observed differences originated from chlorpyrifos and not the inert formulation components.

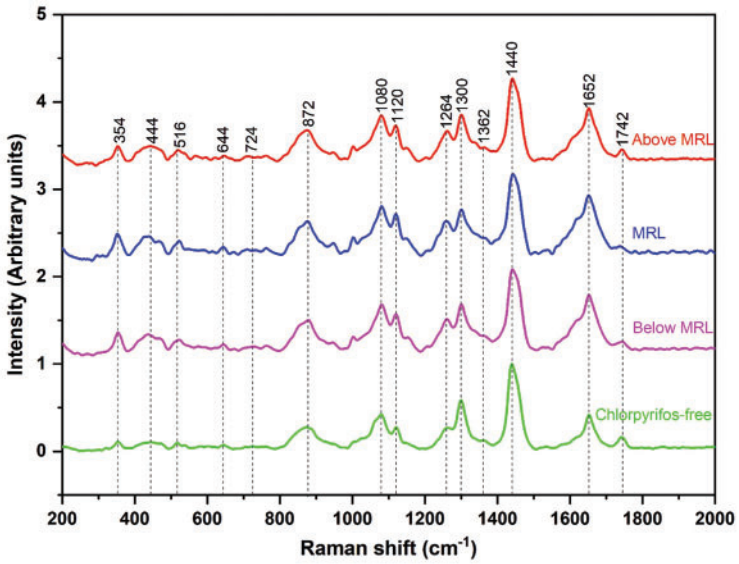

Fig. 1. Plot showing the common bands in the average spectra of the control sample (chlorpyrifos-free milk) and samples spiked with chlorpyrifos at 0.003 ppm (below MRL), 0.01 ppm (MRL), and 0.03 ppm (above MRL).

TABLE I: Attribution of Raman Bands from Milk

Band position (cm^{-1})	Assignment	Component	Reference
354 & 444	C–C	Lactose	[27]
516	Glucose	Lactose	[48]
644	Tyrosine	Protein	[23]
724	ν(C–S)	Protein	[48]
872	phospholipids	Fat	[43]
1080	ν(C–C)	Lactose	[27]
1120	ν(C–C)	Fat	[49]
1264	Amide III	Protein	[27]
1300	$\delta(CH_2)$ twisting	Fat	[46]
1362	Tryptophan	Protein	[23]
1440	$\delta(CH_2)$ scissoring	Fat	[43]
1652	ν(C=C)	Fat	[43]
1742	ν(C=O)	Fat	[27]

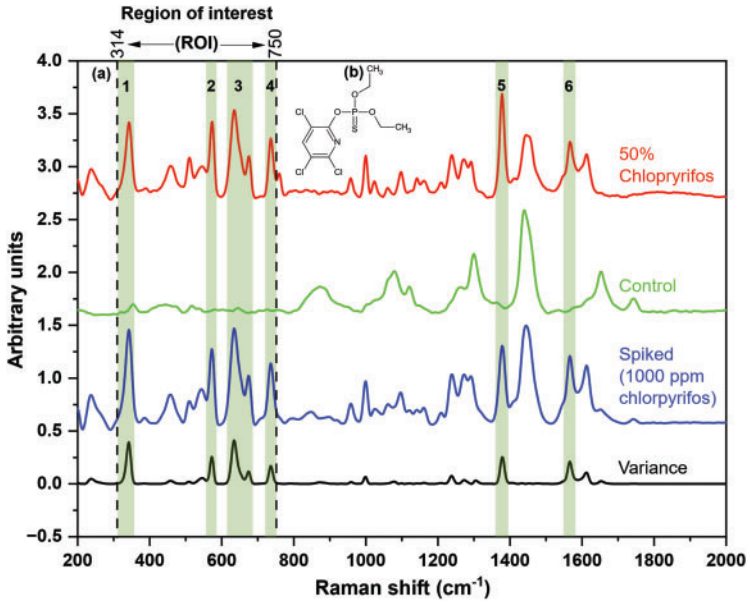

Fig. 2. (a) ANOVA plot showing the bands with significant variance between control and 1000 ppm samples, with the 50% chlorpyrifos reference for comparison (b) Chemical structure of Chlorpyrifos showing its bond and atom arrangement (inset).

Bands with variance above a 30% threshold were considered significant and are marked as striped regions 1–6 in Fig. 2a. Centered at 342, 572, 634, 736, 1378, and 1568 cm^{-1}, these bands showed substantial differences between the control and chlorpyrifos-treated samples, making them potential chlorpyrifos marker bands. To ensure that these spectral features corresponded to chlorpyrifos rather than the inactive ingredients in the commercial pesticide, we cross-referenced them with previously reported Raman studies. The alignment of these bands with the established literature values supports their reliability as characteristic chlorpyrifos signatures.

The chemical structure of chlorpyrifos, illustrated in Fig. 2b, enables the tentative assignment of these bands to specific vibrational modes of the functional groups within the molecule. The Raman band centered at 342 cm^{-1}, consistent with previous studies on chlorpyrifos and related organochlorines, corresponds to C–Cl stretching vibrations [22], [29], [50]–[54]. Similarly, the bands at 572 cm^{-1} and 634 cm^{-1}, attributable to ν(P=S) vibrations, have been reported across multiple pesticide-related Raman investigations [29], [51]–[53], [55]–[59]. The band at 736 cm^{-1} is assigned to P–O–C vibrations, which is consistent with previous spectral interpretations [30], [57]. Additionally, a band near 1378 cm^{-1}, reported in related studies [53], [57], [59], [60], is associated with antisymmetric C=C stretching. Finally, the band observed at 1568 cm^{-1} aligns with prior findings [53], [56], [57], [59], [60], and is attributed to C–H wagging vibrations. The agreement of these spectral features with the established literature supports their assignment to chlorpyrifos rather than to inactive formulation components.

Among the identified bands, the most pronounced spectral differences were observed within the 314–750 cm^{-1} region, which included bands 1–4. This region showed the highest statistical significance in variance analysis and contained new, well-isolated bands that were absent in the control spectra. The strong spectral contrast within this range, corroborated by both statistical analysis and reference spectra, identified it as the region of interest (ROI) for subsequent analyses targeting chlorpyrifos detection.

3.3. PCA of Control, High Concentration, and Low Concentration Groups

While ANOVA was effective in identifying potential marker bands that distinguished between control and chlorpyrifos-treated samples, PCA was applied to further assess the discriminatory power of the ROI, especially at chlorpyrifos concentrations near the MRL. PCA also enabled evaluation of whether a single Raman band within the ROI could reliably distinguish milk samples with trace-level chlorpyrifos contamination.

Fig. 3 shows the PCA results derived from the ROI. The scores plot (Fig. 3a) demonstrates that the ROI facilitates effective separation between the control and 1000 ppm chlorpyrifos-treated samples. The first two PCs (PC1 and PC2) together accounted for over 98% of the total spectral variance, indicating that most of the meaningful variation associated with chlorpyrifos contamination was captured within these components. The corresponding loading plot (Fig. 3b) highlights the specific wavenumber intervals that contributed most significantly to the observed group separation along

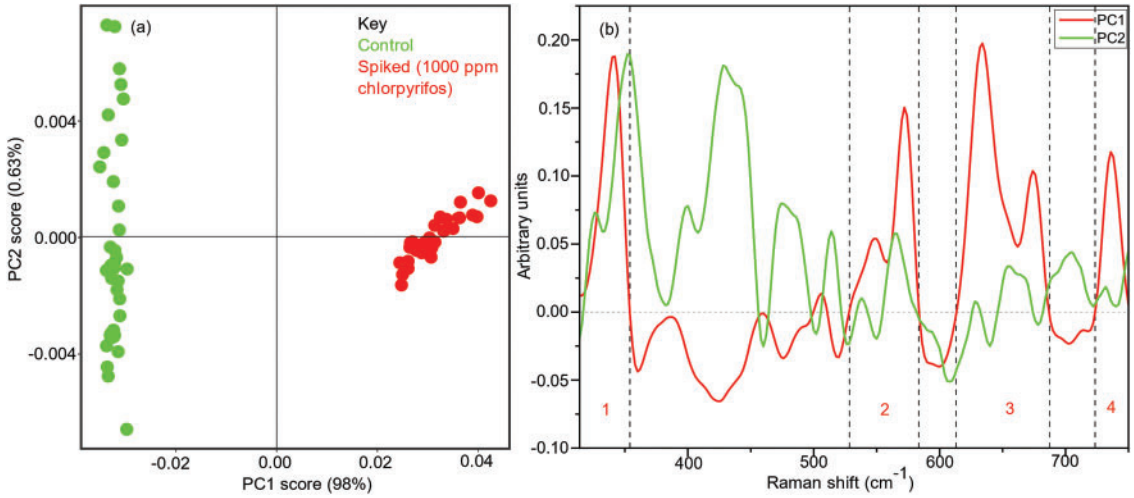

Fig. 3. (a) PCA scores plot and (b) loadings plot for control milk and milk spiked with 1000 ppm chlorpyrifos, based on the ROI (314–750 cm^{-1}).

PC1. These include: (**1**) 314–354, (**2**) 558–584, (**3**) 618–658, and (**4**) 720–750 cm^{-1}. These intervals closely corresponded to the bands previously identified through ANOVA, thereby reinforcing their significance as potential marker bands for chlorpyrifos detection in milk.

While the ROI performs well for high 1000 ppm concentration, practical food safety assessments often focus on detecting low residue levels near the regulatory threshold of 0.01 ppm. Therefore, PCA was applied to assess whether the ROI could reliably differentiate samples at concentrations below the MRL (0.003 ppm), MRL (0.01 ppm), and above MRL (0.03 ppm). To establish a comparative baseline and highlight the advantages of targeted detection using spectral fingerprints, PCA was performed on both the entire spectral range (200–2000 cm^{-1}) and the ROI (314–750 cm^{-1}). The results, presented in Fig. 4, illustrate the relative effectiveness of each approach in discriminating low-concentration chlorpyrifos contamination.

Fig. 4a presents the PCA scores plot based on the full Raman spectral range (200–2000 cm^{-1}), where PC1 and PC2 explain a cumulative variance of over 86%, with PC1 accounting for 80% of the total variance and PC2 contributing an additional 6%. Despite the high level of explained variance, the three groups were not distinctly separated, as evidenced by the substantial overlap between the score clusters. This outcome suggests that a significant portion of the captured variance arises from non-informative fluctuations, which are likely attributable to background signals and variability inherent in the milk matrix. The corresponding loading plot (Fig. 4c) supports this interpretation, showing a broad distribution of loading values across the entire spectrum, with no dominant spectral region clearly driving the group differentiation. This diffuse variance pattern indicates that irrelevant spectral fluctuations likely arising from the milk matrix itself exert a stronger influence on the PCA outcome than chlorpyrifos-specific features of interest.

In contrast, Fig. 4b shows improved separation when PCA was applied to the ROI (314–750 cm^{-1}), particularly between the above MRL (0.03 ppm) and MRL (0.01 ppm) groups. Although the first two PCs in this analysis explain a lower cumulative variance (53%, with PC1 contributing 38% and PC2 contributing 15%), this variance is more analytically relevant because it reflects features associated with chlorpyrifos rather than the matrix background. Some overlap persisted between the below-MRL group (0.003 ppm) and other groups, indicating the challenge of discriminating trace-level contamination and the potential need for additional refinement. The corresponding loading plot (Fig. 4d) confirmed that specific spectral bands within the ROI were responsible for the observed group separation. The most influential wavenumber ranges identified by pronounced positive or negative loadings include 314–354 cm^{-1}, 558–584 cm^{-1}, 618–658 cm^{-1}, and 720–750 cm^{-1}. These intervals aligned with those identified through both ANOVA and earlier PCA (Fig. 3b), reinforcing their reliability as marker bands for chlorpyrifos detection.

While PC3 was also evaluated in both analyses, it contributed only to a marginal increase in explained variance (2% for the full spectrum and 4% for the ROI) and did not enhance group separation. These additional components are likely to reflect residual noise rather than informative variations. Consequently, the first two PCs were deemed sufficient to capture the spectral variation most relevant to chlorpyrifos concentration, while maintaining model interpretability and avoiding overfitting.

To further optimize the group differentiation, PCA was independently applied to each of the four spectral bands within the ROI. For the control and 1000 ppm chlorpyrifos-treated groups, the evaluation criteria included the percentage of variance explained by PC1 and rate of spectral

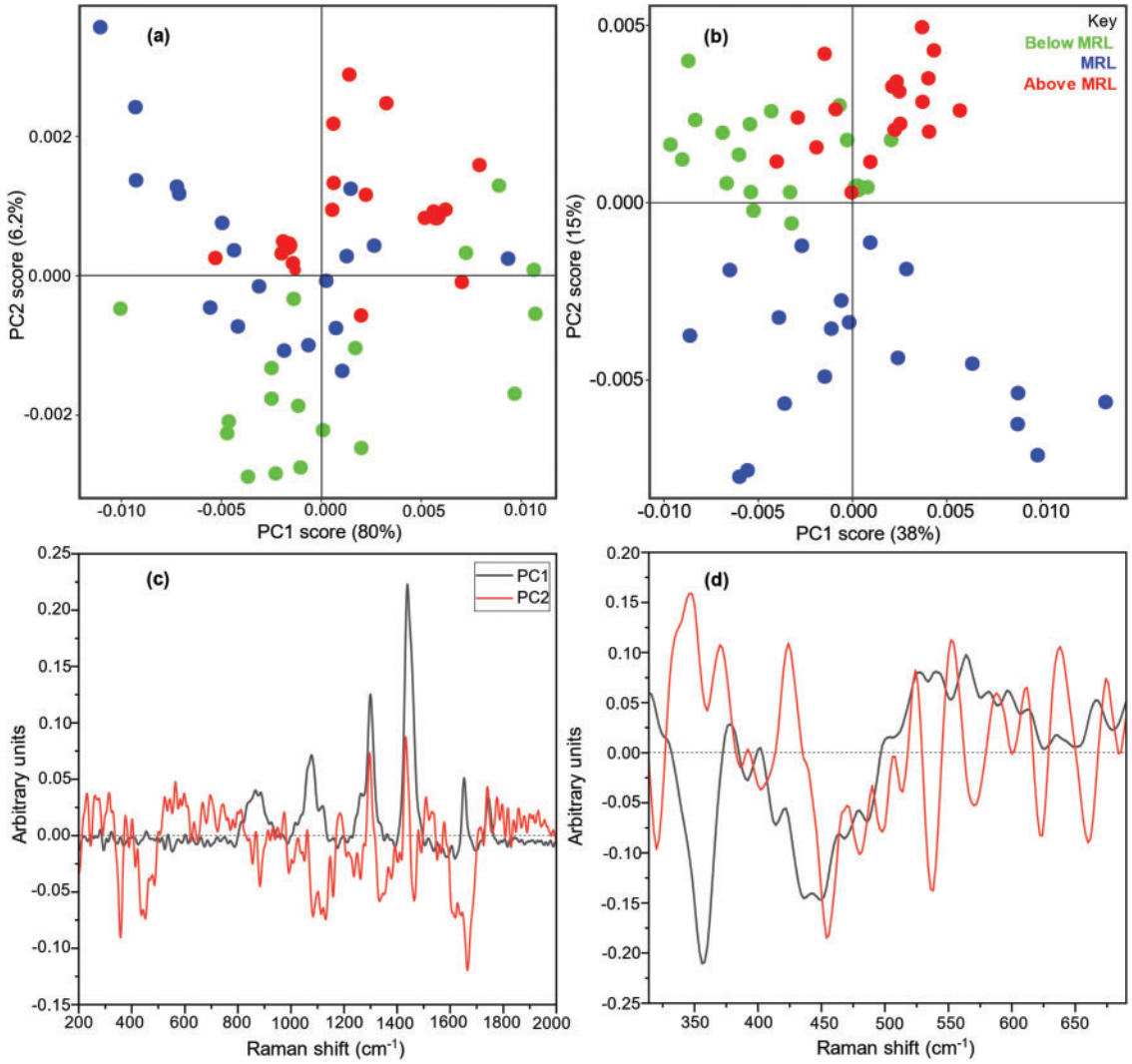

Fig. 4. PCA of Raman spectra for chlorpyrifos-spiked milk samples. (a) PCA score plot based on the entire spectral range (200–2000 cm^{-1}), illustrating the challenge of separating low-concentration groups. (b) PCA score plot based on the ROI (314–750 cm^{-1}), showing improved but still limited group separation. Corresponding PCA loadings plots for (c) the entire spectral range and (d) the ROI.

mis-classification. In contrast, for the low-concentration samples (0.003, 0.01, and 0.03 ppm), band performance was assessed using three criteria: variance explained by PC1, cumulative variance of the first two PCs, and degree of visual separation observed in the PCA score plots.

Visual separation was qualitatively classified into three categories: clear (distinct, non-overlapping clusters representing different groups), poor (substantial cluster overlap, making distinction difficult), and no separation (complete mixing of groups with no discernible boundaries). For all four bands, PC1 accounted for more than 83% of the total spectral variance, and in the case of the control and 1000 ppm groups, all spectra were correctly classified based on the presence or absence of chlorpyrifos. These results support the suitability of all four spectral regions as candidate molecular fingerprints for the detection of chlorpyrifos in milk. A detailed summary of the PCA performance across the control, high-concentration, and low-concentration groups is provided in Table II.

Among the spectral bands examined, the 314–354 cm^{-1} region demonstrated the strongest discriminatory performance. When comparing the control and 1000 ppm chlorpyrifos-treated samples, this band yielded the highest variance along PC1, accounting for 88% of the total spectral variance. The low-concentration samples also exhibited the greatest variance along PC1 (64%) and the highest cumulative variance across the first two PCs (83%), as shown in Fig. 5. These cumulative variance values surpassed those of the other candidate bands: 558–584 cm^{-1} (65%), 618–658 cm^{-1} (52%), and 720–750 cm^{-1} (82%). Notably, the 314–354 cm^{-1} band effectively differentiated between the below-MRL, MRL, and above-MRL sample groups, forming distinct clusters in the PCA scores plots. In contrast, the remaining bands resulted in a substantial overlap between groups, limiting their utility for classification at trace contamination levels. These findings highlight the 314–354 cm^{-1} band as the

TABLE II: PCA Results for Control and High-Concentration Groups as well as the Below MRL, MRL, and above MRL, using the Bands Constituting the ROI and those Obtained from ANOVA

		ROI		ROI & ANOVA-identified bands		
		Control and 1000 ppm groups		Low concentration groups		
	Band (cm^{-1})	Explained variance PC1 (%)	No. of spectra wrongly grouped	Explained variance (%)		Quality of visual separation
				PC1	Cumulative	
1	314–354	88	0	64	83	Clear separation
2	558–584	86	0	37	65	No separation
3	618–658	86	0	32	52	Poor separation
4	720–750	83	0	57	82	No separation
5	1362–1396	–	–	45	78	No separation
6	1550–1584	–	–	59	76	No separation

Note: Separation types are defined as clear (distinct, non-overlapping clusters), poor (substantial overlap with limited distinction), and no separation (complete mixing with no discernible boundaries).

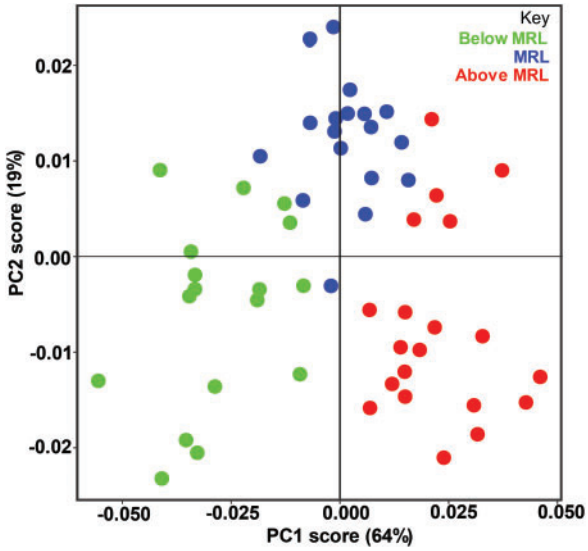

Fig. 5. PCA scores plot showing the precise discrimination of below MRL, MRL, and above MRL samples using the fingerprint (314–354 cm^{-1} band).

most promising spectral fingerprint for the reliable, concentration-sensitive detection of chlorpyrifos in milk.

The superior performance of this band is attributed to the vibrational mode associated with the C–Cl bond, which is a structural feature unique to chlorpyrifos. This chemically distinct bond generates a well-defined Raman signal within the identified fingerprint region, thereby enhancing variance and enabling effective differentiation across varying contamination levels. As illustrated in Fig. 5, PC1 effectively captured the concentration gradient of chlorpyrifos across the samples with increasing concentrations from left to right along the PC1 axis. Samples spiked below the MRL (0.003 ppm) cluster on the negative side of PC1, those spiked above the MRL (0.03 ppm) cluster on the positive side, and samples at the MRL (0.01 ppm) lie between the two. This spatial arrangement confirms that the 314–354 cm^{-1} band enables stratified classification based on the chlorpyrifos content.

To further validate these findings, an alternative approach was employed that focused on low-concentration samples (below the MRL, MRL, and above MRL). Spectral bands exhibiting significant variance across the entire Raman range, as identified by the ANOVA, were analyzed. These regions included: (**1**) 314–354, (**2**) 558–584, (**3**) 618–658, (**4**) 720–750, (**5**) 1362–1396, and (**6**) 1550–1584 cm^{-1} (see Fig. 2a). The PCA results for the first four bands are consistent with those obtained from the initial ROI analysis. However, the inclusion of additional bands (1362–1396 and 1550–1584 cm^{-1}), which emerged only in the full-spectrum ANOVA, did not improve group separation at low chlorpyrifos concentrations, as evidenced by the results summarized in Table II. Based on its consistently high variance, strong group differentiation, and performance across multiple validation approaches, the 314–354 cm^{-1} band was identified as the most precise spectral discriminator. Therefore, this band qualifies as a molecular fingerprint of chlorpyrifos in the context of milk contamination detection.

3.4. Comparison with Previous Studies

Our approach to the detection of chlorpyrifos residues in milk represents a significant departure from earlier studies that employed Raman spectroscopy in conjunction with chemometric methods. Prior research has primarily relied on full-spectrum analysis or broad spectral regions, which often incorporate non-specific features unrelated to the analyte of interest. This inclusion of irrelevant spectral variations can compromise the detection accuracy, particularly at trace concentrations. In contrast, our method systematically identified and validated the most informative Raman bands of chlorpyrifos, enabling precise differentiation, even at low concentrations.

For example, Du *et al*. [29] applied Raman spectroscopy combined with random forest regression to detect chlorpyrifos on pear surfaces, using the full spectral range of 200–800 cm^{-1}. While their model achieved a high coefficient of determination ($R^2 = 0.9003$) for the training set, its performance declined for the test set ($R^2 = 0.8495$), indicating reduced generalization accuracy. This study also reported spectral interference from natural fruit components, which complicated the identification and quantification of chlorpyrifos. Moreover, the model struggled to detect concentrations as high as 0.09 g/kg (90 ppm), underscoring the limitations of broad-spectrum approaches in capturing relevant chemical signals.

Similarly, Tao *et al*. [30] employed SERS to detect pesticide residues on tomato peels, targeting two narrow spectral regions (580–630 cm^{-1} and 660–690 cm^{-1}). However, their study did not comprehensively examine the full Raman spectrum, potentially overlooking additional marker bands that are critical for robust chlorpyrifos detection. Their reported detection limit of 80 ng/cm^2 (0.08 ppm) exceeded the MRL, suggesting the limited sensitivity of the method at regulatory thresholds. Chen *et al*. [55] explored pesticide detection on fruit surfaces using SERS coupled with deep learning algorithms. The spectral analysis was confined to two broad regions: 500–700 cm^{-1} and 950–1300 cm^{-1}. This broad spectral coverage introduced substantial overlap among vibrational features; for instance, the chlorpyrifos-associated band at 609 cm^{-1} coincided with signals from other chemical residues, reducing detection specificity. Although the lowest reported detection limit for chlorpyrifos was 2.1×10^{-4} mg/cm^2 (0.189 ppm), this value remained well above the regulatory threshold of 0.01 ppm, again highlighting the challenges of non-targeted spectral strategies.

Collectively, these studies demonstrate the inherent difficulties associated with full-spectrum or limited-range spectral analyses, either owing to spectral overlap or the omission of critical vibrational information. By contrast, our study adopted a systematic approach that initially evaluated the entire Raman spectrum and then isolated the most discriminative fingerprint bands. This targeted strategy substantially reduced the spectral interference and enabled the successful detection of chlorpyrifos residues below the MRL (0.01 ppm). By refining spectral analysis and focusing on the most chemically specific vibrational feature, our method offers a more accurate, reliable, and selective framework for pesticide residue detection in complex biological matrices such as milk. Furthermore, unlike previous studies that relied on pure analytical-grade standards, which are often expensive and inaccessible in resource-limited settings, our approach demonstrated that commercially available pesticide formulations, when validated against established spectral references, offer a reliable and cost-effective alternative for molecular identification. This strategy not only reduces operational costs but also enhances the scalability of Raman spectroscopy for routine pesticide residue analysis.

4. Conclusion

This study demonstrates the effectiveness of Raman spectroscopy coupled with chemometric techniques for rapid and accurate detection of low-level chlorpyrifos residues in milk. Through the application of one-way ANOVA, we identified key Raman bands exhibiting statistically significant variance between the control and treated samples, specifically those centered at 342, 572, 634, 736, 1378, and 1568 cm^{-1}. The results showed that reliance on the full spectral range introduces non-specific features, that can obscure low-concentration chlorpyrifos signals. This limitation highlights the importance of precise molecular fingerprinting for enhancing detection specificity and analytical robustness. Among the identified spectral bands, the Raman band at 314–354 cm^{-1} emerged as the most reliable molecular fingerprint for chlorpyrifos. This band, attributed to the C–Cl stretching vibrations unique to the chlorpyrifos molecule, consistently enabled discrimination across contamination levels, including samples below the MRL (0.01 ppm). PCA further confirmed its effectiveness, with spiked samples forming distinct clusters according to the contamination level, thereby validating the band's suitability for trace-level detection. These findings support a targeted spectral analysis framework that minimizes interference and improves the detection accuracy for pesticide residues in complex biological matrices. Future work should explore the integration of machine learning techniques to develop classification and regression models based on the identified fingerprint band. Moreover, expanding the molecular

fingerprint library to include additional organophosphorus pesticides would broaden the scope of this method for comprehensive food safety surveillance. Real-world validation across a range of food matrices, including processed dairy products, fruits, and vegetables, is essential for assessing the practical utility and generalizability of the approach.

Data Availability

The data supporting the findings of this study are available from the corresponding author upon reasonable request.

Conflict of Interest

The authors have no conflict of interest to declare.

Funding

We acknowledge the Swedish International Development Cooperation Agency (SIDA), through the International Science Programme (ISP), Uppsala University, for financial support through the ISP KEN:04 project. We also extend our appreciation to the Kenya Education Network for their financial support of this project through the SIG grant number KENET/CMMS/2022/2.

References

[1] Adum AN, Gicharu G, Chimbevo LM, Oshule PS, Essuman S, Asamba MN. Detection and quantification of chlorpyrifos in soil, milk, dip wash, spray race residues using high performance liquid chromatography in selected dairy farms in Kenya. *Sci J Anal Chem*. 2021;9(4):88–95. doi: 10.11648/j.sjac.20210904.12.

[2] Villar D, Schaeffer DJ. Chlorpyrifos should be banned in agriculture and livestock production in Colombia. *Colomb J Anim Sci Vet Med*. 2022;35(2):61–7. doi: 10.17533/udea.rccp.v35n2a7.

[3] Byrne SL, Pinkerton SL. The effect of cooking on chlorpyrifos and 3,5,6-trichloro-2-pyridinol levels in chlorpyrifos-fortified produce for use in refining dietary exposure. *J Agric Food Chem*. 2004;52(25):7567–73. doi: 10.1021/jf049212w.

[4] Singh BK, Walker A, Morgan JA, Wright DJ. Effects of soil pH on the biodegradation of chlorpyrifos and isolation of a chlorpyrifos-degrading bacterium. *Appl Environ Microbiol*. 2003;69(9):5198–206. doi: 10.1128/aem.69.9.5198-5206.2003.

[5] Wołejko E, Łozowicka B, Jabłońska-Trypuć A, Pietruszyńska M, Wydro U. Chlorpyrifos occurrence and toxicological risk assessment: a review. *Int J Environ Res Public Health*. 2022;19(19):12209. doi: 10.3390/ijerph191912209.

[6] Lee K, Yarbrough D, Kozman M, Herrman T, Park J, Wang R, *et al.* Sensitive SERS characterization and analysis of chlorpyrifos and aldicarb residues in animal feed using gold nanoparticles. *J Regul Sci*. 2020;8:1–14. doi: 10.21423/jrs-v08lee.

[7] Rauh VA, Garfinkel R, Perera FP, Andrews HF, Hoepner L, Barr DB, *et al.* Impact of prenatal chlorpyrifos exposure on neurodevelopment in the first 3 years of life among inner-city children. *Pediatrics*. 2006;118(6):e1845–59. doi: 10.1542/peds.2006-0338.

[8] European Union. Commission Regulation (EU) 2020/1085 of 23 July 2020 amending Annexes II and V to Regulation (EC) No 396/2005 of the European Parliament and of the Council as regards maximum residue levels for chlorpyrifos and chlorpyrifos-methyl in or on certain products. *Off J Eur Union*. 2020;63:7–8.

[9] Dasriya V, Joshi R, Ranveer S, Dhundale V, Kumar N, Raghu HV. Rapid detection of pesticide in milk, cereal and cereal based food and fruit juices using paper strip-based sensor. *Sci Rep*. 2021;11(1):18855. doi: 10.1038/s41598-021-96999-w.

[10] Dallegrave A, Pizzolato TM, Barreto F, Bica VC, Eljarrat E, Barceló D. Residue of insecticides in foodstuff and dietary exposure assessment of Brazilian citizens. *Food Chem Toxicol*. 2018;115:329–35. doi: 10.1016/j.fct.2018.03.028.

[11] Shaker EM, Elsharkawy EE. Organochlorine and organophosphorus pesticide residues in raw buffalo milk from agroindustrial areas in Assiut. *Egypt J Dairy Vet Anim Res*. 2015;2(5):172–7. doi: 10.15406/jdvar.2015.02.00049.

[12] Hongsibsong S, Prapamontol T, Xu T, Hammock BD, Wang H, Chen ZJ, *et al.* The organophosphate pesticide chlorpyrifos was monitored in vegetable samples from local markets in northern Thailand by developed immunoassay. *Int J Environ Res Public Health*. 2020;17(13):4723. doi: 10.3390/ijerph17134723.

[13] Ndung'u CN, Kaniu MI, Wanjohi JM, Odongo KO, Kiruri LW, Kaduki KA. Feasibility for rapid on-site screening of pesticide residues in fresh produce using machine learning-assisted diffuse reflectance spectroscopy. *Food Humanit*. 2024;2:100204. doi: 10.1016/j.foohum.2023.100204.

[14] Hackshaw KV, Miller JS, Aykas DP, Rodriguez-Saona L. Vibrational spectroscopy for identification of metabolites in biologic samples. *Molecules*. 2020;25(20):4725. doi: 10.3390/molecules25204725.

[15] Esmonde-White KA, Cuellar M, Lewis IR. The role of Raman spectroscopy in biopharmaceuticals from development to manufacturing. *Anal Bioanal Chem*. 2021;414(2):969–91. doi: 10.1007/s00216-021-03727-4.

[16] Ikedi RI, Birech Z, Kaniu MI. Rapid assessment of molasses adulterated honey using laser Raman spectroscopy and principal component analysis. *Food Anal Methods*. 2023;16(11–12):1702–10. doi: 10.1007/s12161-023-02538-w.

[17] Lin YK, Leong HY, Ling TC, Lin DQ, Yao SJ. Raman spectroscopy as process analytical tool in downstream processing of biotechnology. *Chin J Chem Eng*. 2021;30:204–11. doi: 10.1016/j.cjche.2020.12.008.

[18] Furini LN, Sanchez-Cortes S, López-Tocón I, Otero JC, Aroca RF, Constantino CJ. Detection and quantitative analysis of carbendazim herbicide on Ag nanoparticles via surface-enhanced Raman scattering. *J Raman Spectrosc*. 2015;46(11):1095–101. doi: 10.1002/jrs.4737.

[19] Bowley HJ, Gardiner DJ, Graves PR. *Practical Raman spectroscopy*. 1st ed. Berlin: Springer; 1989.

[20] Ondieki AM, Birech Z, Kaduki KA, Mwangi PW, Mwenze NM, Juma M, *et al.* Fabrication of surface-enhanced Raman spectroscopy substrates using silver nanoparticles produced by laser ablation in liquids. *Spectrochim Acta A Mol Biomol Spectrosc*. 2023;296:122694. doi: 10.1016/j.saa.2023.122694.

[21] Saletnik A, Saletnik B, Puchalski C. Overview of popular techniques of Raman spectroscopy and their potential in the study of plant tissues. *Molecules*. 2021;26(6):1537. doi: 10.3390/molecules26061537.

[22] Ndung'u CN, Kaduki KA, Kaniu IM, Kiruri LW. Enhanced detection of pesticide residues using two-dimensional Raman correlation spectroscopy and machine learning. *Appl Spectrosc Pract*. 2024;2(4):1–11. doi: 10.1177/27551857241303466.
[23] Kuhar N, Sil S, Verma T, Umapathy S. Challenges in application of Raman spectroscopy to biology and materials. *RSC Adv*. 2018;8(46):25888–908. doi: 10.103Du9/c8ra04491k.
[24] Odongo KO, Kaniu MI, Ndung'u CN, Wanjohi JM. Direct and rapid screening of calcium carbide in ripened bananas using chemometrics-assisted laser Raman spectroscopy. *Appl Phys B*. 2023;129:84. doi: 10.1007/s00340-023-08023-w.
[25] Rohman A, Windarsih A, Lukitaningsih E, Rafi M, Betania K, Fadzillah NA. The use of FTIR and Raman spectroscopy in combination with chemometrics for analysis of biomolecules in biomedical fluids: a review. *Biomed Spectrosc Imaging*. 2020;8(3–4):55–71. doi: 10.3233/bsi-200189.
[26] Petersen M, Yu Z, Lu X. Application of Raman spectroscopic methods in food safety: a review. *Biosensors*. 2021;11(6):187. doi: 10.3390/bios11060187.
[27] Khan HMH, McCarthy U, Esmonde-White K, Casey I, O'Shea N. Potential of Raman spectroscopy for in-line measurement of raw milk composition. *Food Control*. 2023;152:109862. doi: 10.1016/j.foodcont.2023.109862.
[28] Zhang S, Qi Y, Tan SP, Bi R, Olivo M. Molecular fingerprint detection using Raman and infrared spectroscopy technologies for cancer detection: a progress review. *Biosensors*. 2023;13(5):557. doi: 10.3390/bios13050557.
[29] Du X, Wang P, Fu L, Liu H, Zhang Z, Yao C. Determination of chlorpyrifos in pears by Raman spectroscopy with random forest regression analysis. *Anal Lett*. 2019;53(6):821–33. doi: 10.1080/00032719.2019.1681439.
[30] Tao M, Fang H, Feng X, He Y, Liu X, Shi Y, *et al.* Rapid trace detection of pesticide residues on tomato by surface-enhanced Raman spectroscopy and flexible tapes. *J Food Qual*. 2022;2022:1–10. doi: 10.1155/2022/6947775.
[31] Blais HN, Schroën K, Tobin JT. A review of multistage membrane filtration approaches for enhanced efficiency during concentration and fractionation of milk and whey. *Int J Dairy Technol*. 2022;75(4):749–60. doi: 10.1111/1471-0307.12884.
[32] Mistry VV, Maubois JL. Application of membrane separation technology to cheese production. In *Cheese: Chemistry, Physics and Microbiology*. Elsevier, 2004. doi: 10.1016/s1874-558x(04)80070-8.
[33] Bukasov R, Sultangaziyev A, Kunushpayeva Z, Rapikov A, Dossym D. Aluminum foil vs. gold film: cost-effective substrate in sandwich SERS immunoassays of biomarkers reveals potential for selectivity improvement. *Int J Mol Sci*. 2023;24(6):5578. doi: 10.3390/ijms24065578.
[34] Cui L, Butler HJ, Martin-Hirsch PL, Martin FL. Aluminium foil as a potential substrate for ATR-FTIR, transflection FTIR or Raman spectrochemical analysis of biological specimens. *Anal Methods*. 2016;8(3):481–7. doi: 10.1039/c5ay02638e.
[35] Sultangaziyev A, Akhmetova A, Kunushpayeva Z, Rapikov A, Filchakova O, Bukasov R. Aluminum foil as a substrate for metal enhanced fluorescence of bacteria labelled with quantum dots, shows very large enhancement and high contrast. *Sens Biosens Res*. 2020;28:100332. doi: 10.1016/j.sbsr.2020.100332.
[36] Afseth NK, Segtnan VH, Wold JP. Raman spectra of biological samples: a study of preprocessing methods. *Appl Spectrosc*. 2006;60(12):1358–67. doi: 10.1366/000370206779321454.
[37] Wahl J, Klint E, Hallbeck M, Hillman J, Wårdell K, Ramser K. Impact of preprocessing methods on the Raman spectra of brain tissue. *Biomed Opt Express*. 2022;13(12):6763–78. doi: 10.1364/boe.476507.
[38] Ostertagova E, Ostertag O. Methodology and application of one-way ANOVA. *Am J Mech Eng*. 2013;1(7):256–61. doi: 10.12691/ajme-1-7-21.
[39] R Core Team. *R: A Language and Environment for Statistical Computing*. Vienna: R Foundation for Statistical Computing; 2021. Available from: https://www.R-project.org/.
[40] Hanson BA. An introduction to ChemoSpec. *Cran R Project*. 2024 Feb 3. Available from: https://cran.r-project.org/web/packages/ChemoSpec/vignettes/ChemoSpec.pdf.
[41] Grewal MK, Huppertz T, Vasiljevic T. FTIR fingerprinting of structural changes of milk proteins induced by heat treatment, deamidation and dephosphorylation. *Food Hydrocoll*. 2018;80:160–7. doi: 10.1016/j.foodhyd.2018.02.010.
[42] Contarini G, Povolo M. Phospholipids in milk fat: composition, biological and technological significance, and analytical strategies. *Int J Mol Sci*. 2013;14(2):2808–31. doi: 10.3390/ijms14022808.
[43] Silva MG, de Paula IL, Stephani R, Edwards HGM, de Oliveira LF. Raman spectroscopy in the quality analysis of dairy products: a literature review. *J Raman Spectrosc*. 2021;52(12):2444–78. doi: 10.1002/jrs.6214.
[44] Landi N, Ragucci S, Di Maro A. Amino acid composition of milk from cow, sheep and goat raised in Ailano and Valle Agricola, two localities of 'Alto Casertano' (Campania region). *Foods*. 2021;10(10):2431. doi: 10.3390/foods10102431.
[45] Rafiq S, Huma N, Pasha I, Sameen A, Mukhtar O, Khan MI. Chemical composition, nitrogen fractions and amino acids profile of milk from different animal species. *Asian-Australas J Anim Sci*. 2015;29(7):1022–8. doi: 10.5713/ajas.15.0452.
[46] Yazgan NN, Genis HE, Bulat T, Topcu A, Durna S, Yetisemiyen A, *et al.* Discrimination of milk species using Raman spectroscopy coupled with partial least squares discriminant analysis in raw and pasteurized milk. *J Sci Food Agric*. 2020;100(13):4756–65. doi: 10.1002/jsfa.10534.
[47] Amores G, Virto M. Total and free fatty acids analysis in milk and dairy fat. *Separations*. 2019;6(1):14. doi: 10.3390/separations6010014.
[48] Li JX, Qing CC, Wang XQ, Zhu MJ, Zhang BY, Zhang ZY. Discriminative feature analysis of dairy products based on machine learning algorithms and Raman spectroscopy. *Curr Res Food Sci*. 2024;8:100782. doi: 10.1016/j.crfs.2024.100782.
[49] Amjad A, Ullah R, Khan S, Bilal M, Khan A. Raman spectroscopy based analysis of milk using random forest classification. *Vib Spectrosc*. 2018;99:124–9. doi: 10.1016/j.vibspec.2018.09.003.
[50] Dhakal S, Li Y, Peng Y, Chao K, Qin J. Nondestructive detection of pesticide residue concentration in apple by Raman spectral technology. *2013 ASABE Annual International Meeting*, pp. 131587022, Kansas City, (MO), 2013. doi: 10.13031/aim.20131587022.
[51] Dhakal S, Peng Y, Li Y, Chao K, Qin J, Zhang L, *et al.* Rapid detection of chlorpyrifos pesticide residue concentration in agro-product using Raman spectroscopy. *Proc SPIE*. 2014;9108:91080O-1–91080O-8. doi: 10.1117/12.2050137.
[52] Li Y, Sun Y, Peng Y, Dhakal S, Chao K, Liu Q. Rapid detection of pesticide residue in apple based on Raman spectroscopy. *Proc SPIE*. 2012;8369:83690I-1–83690I-6. doi: 10.1117/12.918527.
[53] Ma P, Wang L, Xu L, Li J, Zhang X, Chen H. Rapid quantitative determination of chlorpyrifos pesticide residues in tomatoes by surface-enhanced Raman spectroscopy. *Eur Food Res Technol*. 2019;246(1):239–51. doi: 10.1007/s00217-019-03408-8.
[54] Zhang X, Zhou Q, Huang Y, Li Z, Zhang Z. Contrastive analysis of the Raman spectra of polychlorinated benzene: hexachlorobenzene and benzene. *Sensors*. 2011;11(12):11510–5. doi: 10.3390/s111211510.
[55] Chen Z, Dong X, Liu C, Wang S, Dong S, Huang Q. Rapid detection of residual chlorpyrifos and pyrimethanil on fruit surface by surface-enhanced Raman spectroscopy integrated with deep learning approach. *Sci Rep*. 2023;13(1):19855. doi: 10.1038/s41598-023-45954-y.
[56] Ngo TC, Trinh QT, Thi Thai An N, Tri NN, Trung NT, Truong DH, *et al.* SERS spectra of the pesticide chlorpyrifos adsorbed on silver nanosurface: the Ag20 cluster model. *J Phys Chem C*. 2020;124(39):21702–16. doi: 10.1021/acs.jpcc.0c06078.
[57] Shende C, Inscore F, Sengupta A, Stuart J, Farquharson S. Rapid extraction and detection of trace chlorpyrifos-methyl in orange juice by surface-enhanced Raman spectroscopy. *Sens Instrum Food Qual Saf*. 2010;4(3–4):101–7. doi: 10.1007/s11694-010-9100-6.

[58] Zhai C, Peng Y, Li Y, Chao K. Extraction and identification of mixed pesticides' Raman signal and establishment of their prediction models. *J Raman Spectrosc*. 2016;48(3):494–500. doi: 10.1002/jrs.5049.
[59] Zhu X, Li W, Wu R, Liu P, Hu X, Xu L, *et al.* Rapid detection of chlorpyrifos pesticide residue in tea using surface-enhanced Raman spectroscopy combined with chemometrics. *Spectrochim Acta A Mol Biomol Spectrosc*. 2021;250:119366. doi: 10.1016/j.saa.2020.119366.
[60] Xu Q, Guo X, Xu L, Ying Y, Wu Y, Wen Y, *et al.* Template-free synthesis of SERS-active gold nanopopcorn for rapid detection of chlorpyrifos residues. *Sens Actuators B Chem*. 2017;241:1008–13. doi: 10.1016/j.snb.2016.11.021.